Photoionization of aligned molecular excited states

J. R. Appling, M. G. White, W. J. Kessler, R. Fernandez, and E. D. Poliakoff

Citation: The Journal of Chemical Physics **88**, 2300 (1988); doi: 10.1063/1.454065
View online: http://dx.doi.org/10.1063/1.454065
View Table of Contents: http://scitation.aip.org/content/aip/journal/jcp/88/4?ver=pdfcov
Published by the AIP Publishing

Photoionization of aligned molecular excited states

J. R. Appling and M. G. White
Chemistry Department, Brookhaven National Laboratory, Upton, New York 11973

W. J. Kessler, R. Fernandez, and E. D. Poliakoff
Department of Chemistry, Boston University, Boston, Massachusetts 02215

(Received 13 August 1987; accepted 30 October 1987)

Photoelectron angular distributions of several excited states of NO have been measured in an effort to better elucidate the role of alignment in resonant multiphoton excitation processes of molecules. In contrast to previous molecular REMPI measurements on NO, (2 + 1) angular distributions taken for low rotational levels of the $E\,^2\Sigma^+$ ($4s\sigma$) Rydberg state of NO exhibit complex angular behavior which is characteristic of strong spatial alignment of the optically prepared levels. Photoelectron angular distributions were also found to be strongly branch and J dependent with the lowest rotational levels of the $R_{21} + S_{11}$ branch exhibiting the full anisotropy expected for an overall three-photon process. Fluorescence anisotropies extracted from complementary two-photon fluorescence angular distribution measurements reveal small, but nonzero alignment in all rotational levels with $J > 1/2$, in contrast to the photoelectron results. Additional photoelectron angular distributions taken for (1 + 1) REMPI via the $A\,^2\Sigma^+$ ($3s\sigma$), $v = 0$ state exhibit near "$\cos^2\theta$" distributions characteristic of photoionization of unaligned target states. The observed photoelectron data are qualitatively interpreted on the basis of the angular momentum constraints of the excitation-induced alignment and photoionization dynamics which determine the observable moments in the angular distribution.

I. INTRODUCTION

Photoelectron angular distribution measurements are of great utility in conventional one-photon VUV photoelectron spectroscopy (PES) as a result of their sensitivity to the dynamics of the photoionization process.[1] These studies can be extended to various excited states of neutral molecules through the application of resonantly enhanced multiphoton ionization (REMPI) techniques. The REMPI process also provides a dynamical probe of photoionization from optically prepared excited levels which are not isotropically distributed relative to the photon beam. Nonstatistical populations of $|JM_J\rangle$ substates (M_J is the space-fixed projection of total angular momentum J) are the result of differences in their multiphoton excitation amplitudes. In principle, photoelectron angular distributions determined with REMPI-PES should be sensitive to this alignment since the photoelectrons are now emitted from nonrandomly oriented target states. Furthermore, photoelectron measurements can probe higher moments of the alignment and thereby provide new information not obtainable from fluorescence polarization experiments.[2-4]

The purpose of the measurements presented here is to investigate systematically the role of excited state alignment in the dynamics of the photoionization step in REMPI of NO. Photoelectron angular distributions in (2 + 1) REMPI and two-photon laser-induced fluorescence (LIF) anisotropies were measured for several rotational levels of the $E\,^2\Sigma^+$ ($4s\sigma$), $v' = 0$ Rydberg state, i.e.,

$$\mathrm{NO}(X\,^2\Pi_{1/2}, v'' = 0, J'') \xrightarrow{2\gamma} \mathrm{NO}^*(E\,^2\Sigma^+, v' = 0, J'), \tag{1}$$

$$\mathrm{NO}^*(E\,^2\Sigma^+, v' = 0, J') \xrightarrow{1\gamma} \mathrm{NO}^+(X\,^1\Sigma^+, v^+ = 0) + e^- \quad (\mathrm{PES}), \tag{2}$$

$$\mathrm{NO}^*(E\,^2\Sigma^+, v' = 0, J') \rightarrow \mathrm{NO}(A\,^2\Sigma^+, v = 0) + \gamma' \quad (\mathrm{LIF}). \tag{3}$$

The LIF angular distribution measurements allow a direct probe of the excitation-induced alignment[5,6] and therefore provide additional insight into the interpretation of the observed photoelectron angular distributions. Additional photoelectron angular distributions were obtained for (1 + 1) REMPI via the $A\,^2\Sigma^+$ ($3s\sigma$), $v = 0$ state in order to compare with recent *ab initio* calculations of Dixit *et al.*[7]

The general form that describes the angular distribution for photoelectrons ejected during an $(n + 1)$-photon REMPI process using a single, linearly polarized laser is given by[8-10]

$$W_e(\theta) \propto \sum_{k=0} a_{2k} P_{2k}(\cos\theta), \tag{4}$$

where the $P_{2k}(\cos\theta)$ are Legendre polynomials of order $2k$ and θ is the angle between the polarization and photoelectron propagation vectors. The a_{2k} coefficients contain information concerning the bound-continuum photoionization dynamics as well as information pertaining to the M_J population distribution of the excited state.[2] For $(n + 1)$ REMPI via spherically symmetric excited states, e.g., $J \leqslant 1/2$, or states depolarized by collisional relaxation, the angular distribution expression reduces to $a_0 + a_2 P_2(\cos\theta)$, where a_2/a_0 is the familiar asymmetry parameter β used in conventional single-photon PES descriptions.[11,12] The appearance of higher order terms in photoelectron angular distributions,

 0021-9606/88/042300-09$02.10

i.e., $k > 1$ in Eq. (4), is the signature of resonant multiphoton ionization via aligned intermediate states. The index k is generally limited to $(n + 1)$, however, angular momentum constraints can reduce the highest observable anisotropy as will be discussed later.

The anisotropy of fluorescence from aligned excited states follows the form[5,6,13]

$$W_\gamma(\theta) \propto 1 - \tilde{\beta}/2 \cdot P_2(\cos\theta) , \tag{5}$$

where $\tilde{\beta}$ is the fluorescence anisotropy parameter (different from the PES asymmetry parameter). The anisotropy index Q is the quantity actually measured and is defined as

$$Q = (I_{90} - I_0)/(I_{90} + I_0) , \tag{6}$$

where I_θ represents the fluorescence intensity measured at an angle θ with respect to the polarization vector of the laser radiation [$\tilde{\beta} = 8Q/(Q + 3)$].

Explicit expressions relating $\tilde{\beta}$ (or Q) to the quadrupole moment of the alignment distribution $A_0^{(2)}$ have been developed from general angular momentum considerations[14–16] and recent two-photon fluorescence studies[13] of the $A\,^2\Sigma^+$, $v = 0$ level of NO confirm the theoretical predictions.[17] Since $A_0^{(2)}$ can be loosely interpreted as the most likely value of $\mathbf{J}\cdot\mathbf{E}$ ($\mathbf{J}$ is the total angular momentum of the intermediate state and $\mathbf{E}$ is the polarization vector),[6] $A_0^{(2)}$ provides a direct measure of the spatial orientation of the excited molecules. Hence, complementary measurements of the fluorescence and photoelectron angular distributions provide a more complete description of the REMPI process by allowing at least a qualitative decoupling of the excitation induced spatial alignment and subsequent ionization dynamics.

II. EXPERIMENTAL

Photoelectron angular distribution measurements were performed at Brookhaven National Laboratory using the time-of-flight (TOF) photoelectron spectrometer system shown schematically in Fig. 1. Laser radiation in the 328.5–329.0 nm region suitable for two-photon excitation of the E, $v' = 0$ state was generated as the frequency doubled output (Quanta Ray WEX) of a pulsed (20 Hz), Nd:YAG-pumped dye laser (Quanta Ray DCR and PDL) containing DCM dye (Exciton). Tunable UV radiation in the range 224–227 nm for $(1 + 1)$ REMPI via the A, $v' = 0$ state was produced by nonlinear mixing of unused 1064 nm pump beam with the frequency doubled output of the dye laser using a Rhodamine 590/610 (Exciton) dye mixture. Output powers are typically in the range of 2–4 mJ/pulse and 500–750 μJ/pulse for the E and A state experiments, respectively, with beams linearly polarized greater than 95%. A Glan polarizing prism ensures 100% polarization purity before the polarization vector of the laser radiation is rotated with a Soleil–Babinet compensator tuned to one-half-wave retardation at specific wavelengths. The laser beam is admitted to the vacuum chamber through a fused silica window after focusing with a 200 mm focal length lens mounted on an XYZ translation stage.

The vacuum chamber housing the photoelectron spectrometer is pumped by a liquid nitrogen-trapped 6 in. diffusion pump which maintains a background pressure of $\sim 3 \times 10^{-7}$ Torr. A 50 l/s turbomolecular pump (Balzers) mounted on the back of the spectrometer provides additional pumping speed for the detector region and flight tube. To reduce the congestion of A and E state ($v' = 0$) rotational spectra, angular distribution measurements were performed on rotationally "cold" NO produced by high pressure expansions (50–100 psi) of a 5% mixture of NO (Matheson,

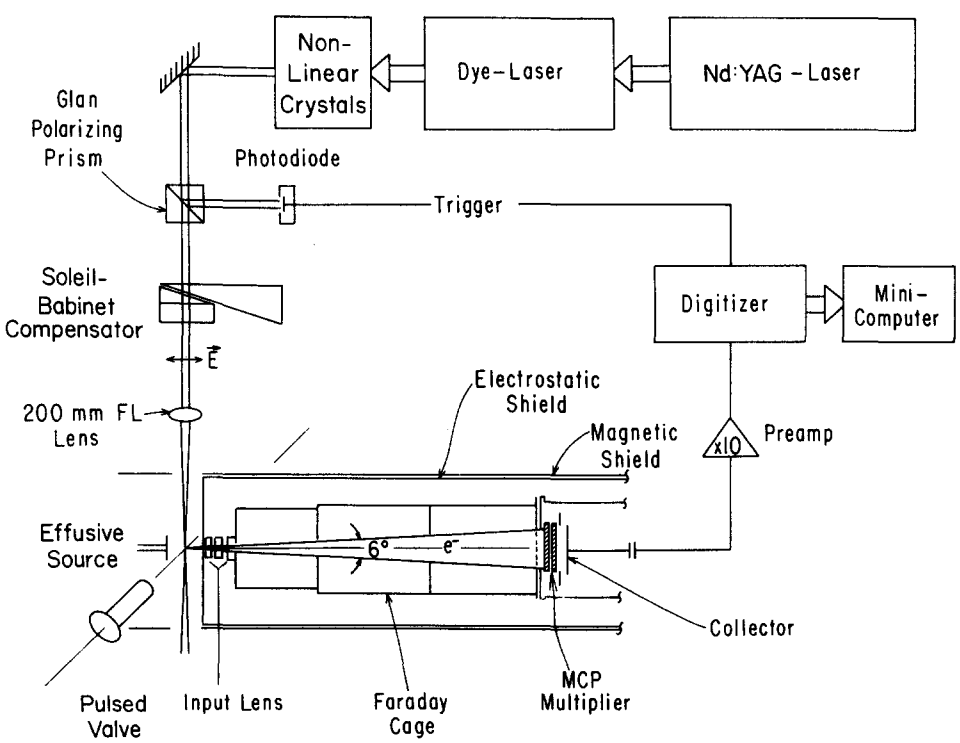

FIG. 1. Schematic of experimental setup. Individual components are discussed in the text.

99.6% purity) in argon. The sample chamber pressure was typically 2×10^{-5} Torr for pulsed molecular beam valve (Newport Corp. BV 1000) operation in the PES apparatus. The NO/Ar gas pulses enter the interaction region of the spectrometer at right angles to both the propagation direction of the laser and the detector axis of the TOF flight tube. A supplementary effusive gas source (70 μm diam. nozzle) attached below the interaction region and facing the 2 mm aperture entrance to the flight tube was used for measurements at higher rotational temperatures. Figure 2 presents the $(2+1)$ E state rotational spectra obtained using both the pulsed valve (top trace) and room temperature effusive source (bottom trace). The branch assignments are based on spectroscopic constants tabulated in the literature.[18] We estimate the rotational temperature of NO produced by the pulsed valve to be approximately 5 K. The rotational temperature was optimized by adjusting the delay between the laser pulse and valve pulse while monitoring the intensity of the $R_{21}+S_{11}$ (1/2) line in the photoelectron spectrum.

For angular distribution measurements, photoelectrons ejected at right angles to the NO gas jet and probe laser were collected ($\sim1\times10^{-3}$ sr) as a function of the angle (θ) formed by the polarization vector of the laser radiation and the detector axis of the TOF spectrometer. A photodiode triggered by the laser pulse provides a time zero for the photoelectron time of flight. A small positive voltage ($+2$ V) was applied to the Faraday cage of the spectrometer to augment the survival rate of photoelectrons which enter the flight tube. This cage voltage increased the overall photoelectron intensities and signal-to-noise level while producing no discernable effect on angular distributions. Representative TOF photoelectron spectra are shown in Fig. 3 for the polarization vector parallel ($\theta=0°$) and perpendicular ($\theta=90°$) to the collection axis of the TOF analyzer. The Rydberg character of the E state is manifested by the presence of a single photoelectron peak corresponding to production of $X\,^1\Sigma^+$ ($v^+=0$) ionic states. Similar photoelectron spectra were obtained for resonant excitation of the A, $v=0$ state. It is then a simple matter to monitor the REMPI photoelectrons in the $v^+=0$ channel for a specific rotational transition in the NO sample as a function of laser polarization angle determined by the Soleil–Babinet compensator. Angular dependence of the photoelectron intensity in the $v^+=0$ channel was recorded for 40 laser shots for each angle incremented by 5° during ten 360° scans. Collection of the digitized output of the multichannel plate detector and control of the Soleil–Babinet stage rotations were accomplished through the use of CAMAC modules (Kinetic Systems 3912 Crate Controller, LeCroy 8828 Transient Recorder, Kinetic Systems 3112 12 bit DAC) interfaced to a PDP 11/23 minicomputer.

Two-photon fluorescence angular distribution measurements via the $E, v'=0$ state were taken at Boston University using the LIF apparatus described in detail elsewhere.[13] The laser system (Quanta-Ray DCR-2A Nd:YAG pump laser) and polarization optics (polarizing prism, Babinet–Soleil compensator) were similar to that described above except for the use of a custom Littman-type dye laser which has significantly better linewidth (0.12 cm^{-1}) than the commercial dye laser (0.4 cm^{-1}) used in the photoelectron measurements. Rotationally cold NO was produced by a cw expansion of a mixture of 10% NO in Ar at 50 psi through a 20 μ diameter nozzle. A baffled 4 in. diffusion pump (Varian VHS-4) added to the LIF chamber provided the additional

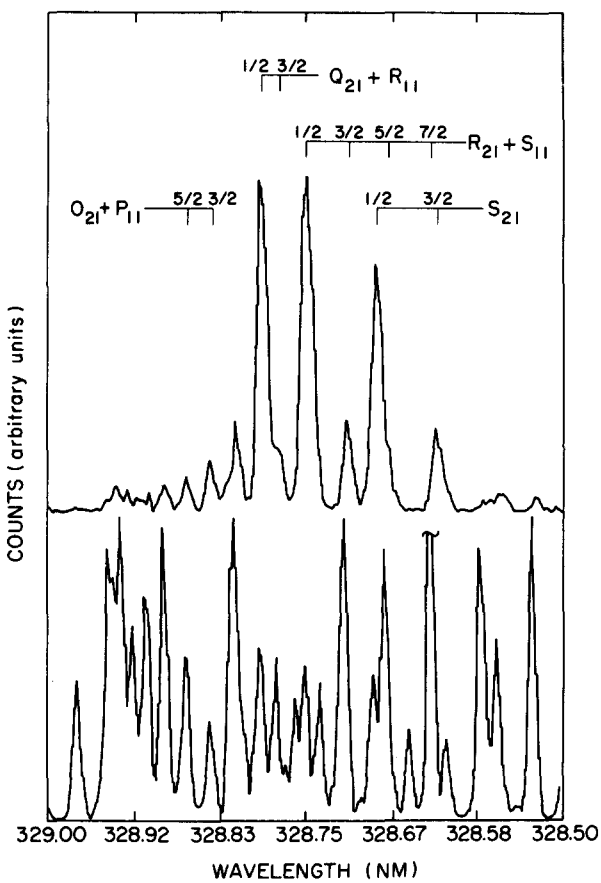

FIG. 2. $(2+1)$ REMPI spectra of the $E\,^2\Sigma^+, v'=0$ state obtained by measuring the $v^+=0$ photoelectron peak intensity as a function of dye laser wavelength. Upper curve: pulsed valve molecular beam source. Lower curve: effusive jet gas source.

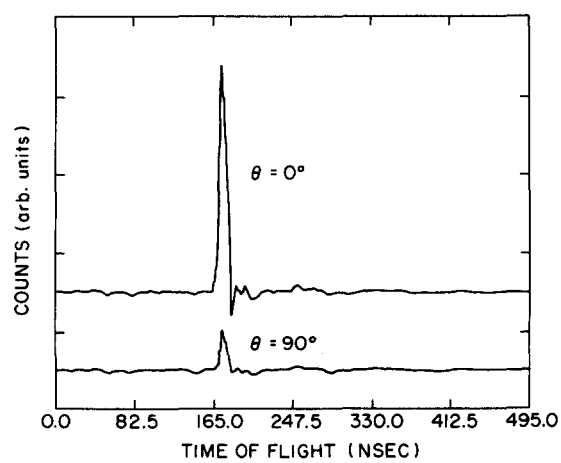

FIG. 3. Time-of-flight photoelectron spectra for $(2+1)$ REMPI of the $E\,^2\Sigma^+, v'=0$ state taken at 0° and 90° relative to the polarization vector of the laser radiation. The single peak corresponds to the $X\,^1\Sigma^+, v^+=0$ final state of the ion.

pumping required for molecular beam studies. Typical operating background pressures were 2×10^{-4} Torr. Fluorescence from the $A\,^2\Sigma^+(v=0)\leftarrow E\,^2\Sigma^+(v'=0)$ transition centered at 600 nm[19] was observed using a narrow band interference filter and detected by a cooled (-30 °C) photomultiplier (Hamamatsu 943-02). The fluorescence anisotropy was obtained by measuring the fluorescence intensity at 0° and 90° relative to the polarization vector of the excitation laser for each rotational line of interest. Fluorescence intensities are measured by charge integration with an *A/D* converter (LeCroy 2249W) which is time gated relative to the *Q*-switch output of the Nd:YAG pump laser. Typical runs involved integrations over several hundred laser pulses for each polarization angle.

III. RESULTS

A. $E\,^2\Sigma^+(4s\sigma)$, $v=0$ state

Measured fluorescence anisotopies for various rotational levels and branches of the two-photon LIF spectrum of rotationally cold $E, v'=0$ NO molecules are presented in Table I. Error bars for the LIF measurements correspond to the average deviation of three separate runs. As expected, anisotropy value for the $P_{11}(3/2)$ line ($J'=1/2$ upper state) is zero within experimental error. The fluorescence anisotropy for the $P_{11}(5/2)$ line is observed to be negative, whereas all other transitions in the Q_{21}, R_{21}, and S_{21} branches exhibit positive values with a general decrease in Q as J increases. Also shown in Table I are theoretical estimates[17] of the fluorescence anisotropy parameters with and without corrections for nuclear hyperfine coupling.[5,6] For the mixed branches ($R_{21}+S_{11}$,$Q_{21}+R_{11}$,$P_{11}+O_{21}$) coherence effects were neglected and the resulting anisotropies represent an incoherent sum of the two spin-doublets weighted by their two-photon rotational line strengths as given by Halpern, Zacharias, and Wallenstein.[20] The inclusion of hyperfine depolarization results in smaller Q values and generally brings the theoretical Q values significantly closer to the experimentally measured anisotropies. One significant exception is the $Q_{21}+R_{11}(1/2)$ line, where the experimental result ($Q_{exp}=0.099$) lies between the calculated value that includes hyperfine depolarization ($Q=0.045$) and that which neglects hyperfine depolarization ($Q=0.158$).

Photoelectron angular distributions for various $E\leftarrow\leftarrow X$,(0,0) excitation branches and low rotational quanta are shown in Figs. 4–6. Angular distributions were least-squares fit to Legendre polynomial expansions of Eq. (4) with $k_{max}=3$, which corresponds to the highest anisotropy allowed for a (2 + 1) REMPI process.[8–10] For purposes of comparison, only normalized angular distributions $1+A_2P_2+A_4P_4+A_6P_6$, where $A_{2k}=a_{2k}/a_0$ are reported. No correction has been made for the finite solid angle of the electron analyzer (±3°). The results for the $P_{11}(3/2)$ transition presented in Fig. 4 correspond to photoionization via an isotropic excited state ($N'=0, J'=1/2$) and the data is well fit by a simple $1+A_2P_2(\cos\theta)$ distribution with $A_2=1.24\pm0.02$. Here, the A_2 coefficient can be directly identified with the β asymmetry parameter used in one-photon photoelectron spectroscopy. The single $Q_{21}+R_{11}$ mixed branch line studied (Fig. 4) exhibits an angular distribution similar to that of the $P_{11}(3/2)$ line with fit coefficients $A_2=1.24\pm0.04$ and $A_4=0.05\pm0.03$. The small admixture of $P_4(\cos\theta)$ character is barely statistically valid for the $Q_{21}+R_{11}(1/2)$ result.

Photoelectron distributions measured for the $R_{21}+S_{11}$ transitions shown in Fig. 5 are in sharp contrast to the "isotropic" nature of the $P_{11}(3/2)$ and $Q_{21}+R_{11}(1/2)$ results. Most striking is the first member of the progression, $R_{21}+S_{11}(1/2)$, which requires a significant amount of both $P_4(\cos\theta)$ and $P_6(\cos\theta)$ to fit the data. The $A_2=1.27\pm0.02$ coefficient is similar to that seen for the $P_{11}(5/2)$, but the angular distribution is necessarily fit by $A_4=-0.27\pm0.02$ and $A_6=-0.38\pm0.02$. A clear trend is exhibited in the $R_{21}+S_{11}$ progression as the amount of $P_4(\cos\theta)$ and $P_6(\cos\theta)$ character decreases steadily from the $J''=1/2$ level to zero at the $J''=7/2$ level. The data for the $R_{21}+S_{11}(7/2)$ transition is fit with the "isotropic" form $1+A_2P_2(\cos\theta)$ with $A_2=1.28\pm0.02$. It is interesting to note that the scatter in the data for the $R_{21}+S_{11}(5/2)$ line obscures the dip at $n\pi/2$, but the analytical fit to the overall shape of the distribution yields a result consistent with the

TABLE I. Photoelectron angular distribution coefficients A_{2k} and fluorescence anisotropies Q for several rotational branch transitions in the (2 + 1) REMPI and two-photon LIF of the $E\,^2\Sigma^+$, $v=0$ state of NO.

	Photoelectron angular distributions[a]			Fluorescence anisotropy, $Q(\times100)$		
					Calculated[b]	
Rotational transition	$A_2(\pm)$	$A_4(\pm)$	$A_6(\pm)$	Expt.($\pm$)	Without hyperfine	With hyperfine
$P_{11}(3/2)$	1.24(0.02)	···	···	0.7(2.1)	0	0
$Q_{21}+R_{11}(1/2)$	1.24(0.04)	0.05(0.03)	···	9.9(1.9)	15.8	4.5
$R_{21}+S_{11}(1/2)$	1.27(0.02)	−0.27(0.02)	−0.38(0.02)	8.2(2.0)	16.7	7.0
$R_{21}+S_{11}(3/2)$	1.23(0.02)	−0.20(0.02)	−0.24(0.02)	5.3(2.0)	11.2	8.0
$R_{21}+S_{11}(5/2)$	1.09(0.02)	−0.14(0.02)	−0.15(0.02)	2.8(2.5)	9.2	7.6
$R_{21}+S_{11}(7/2)$	1.28(0.02)	···	···			
$S_{21}(1/2)$	1.24(0.03)	0.20(0.03)	0.09(0.03)	11.5(2.0)	18.2	10.8
$S_{21}(3/2)$	1.23(0.02)	···	···	9.7(2.0)	16.1	12.2

[a] Normalized coefficient $A_{2k}=a_{2k}/a_0$.
[b] From Ref. 20.

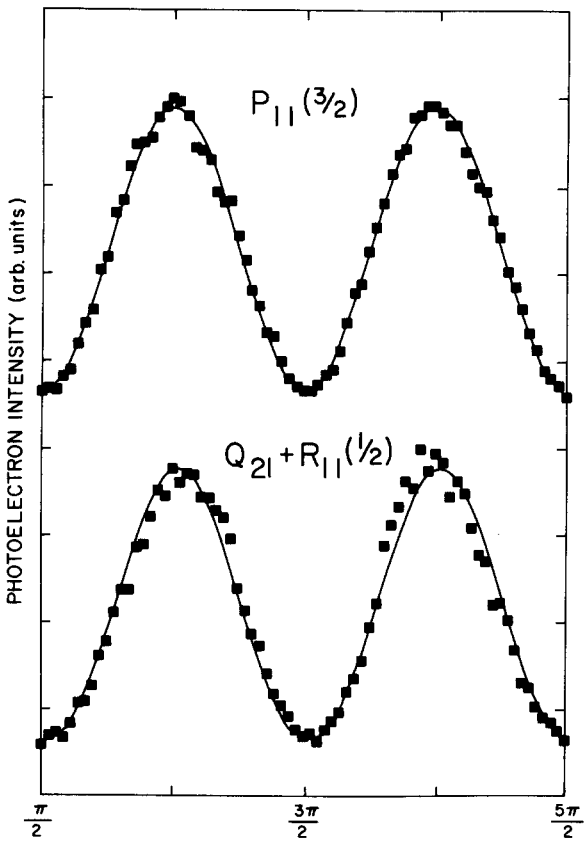

FIG. 4. Photoelectron angular distributions for $(2+1)$ REMPI of the $E\,^2\Sigma^+, v'=0$ state via the $P_{11}(3/2)$ and $Q_{21}+R_{11}(1/2)$ rotational branches. ■ experiment; —least-squares fit to Eq. (4).

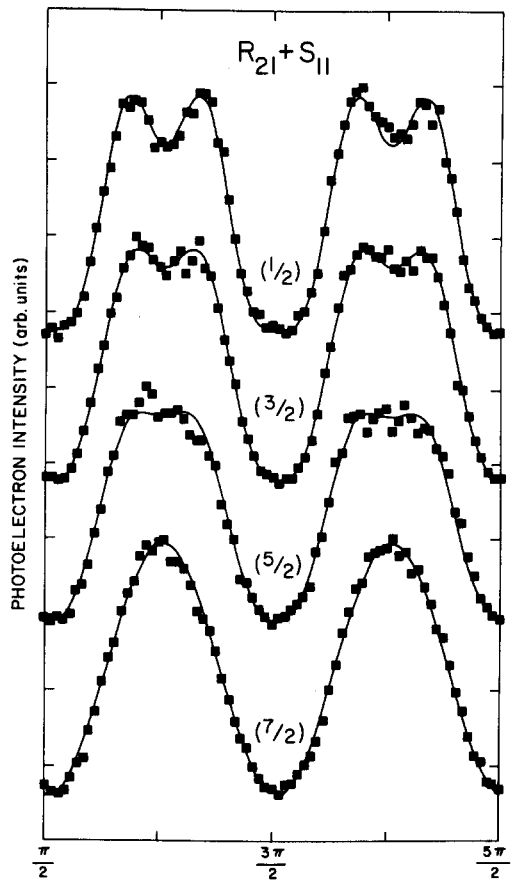

FIG. 5. Photoelectron angular distributions for $(2+1)$ REMPI of the $E\,^2\Sigma^+, v'=0$ state via the first four members of the $R_{21}+S_{11}$ rotational branch. ■ experiment; — least squares fit to Eq. (4).

observed trend.

As shown in Fig. 6, the S_{21} progression reaches the isotropic limit at its second member $S_{21}(3/2)$ with $A_2 = 1.23 \pm 0.02$. The $S_{21}(1/2)$ angular distribution requires contribution from both $P_4(\cos\theta)$ and $P_6(\cos\theta)$, but differs significantly from the $R_{21}+S_{11}$ result at low J''. The higher moment contribution to the description of the $S_{21}(1/2)$ data is in the form of positive P_4 and P_6 coefficients. Thus the $A_4 = 0.20 \pm 0.03$ and $A_6 = 0.09 \pm 0.03$ coefficients produce a fit highly dissimilar to the dips observed for the $R_{21}+S_{11}$ progression. The experimental and theoretical results pertaining to the two-photon LIF and $(2+1)$ REMPI of the E, $v'=0$ state are summarized in Table I.

B. $A\,^2\Sigma^+(3s\sigma)$, $v=0$ state

Photoelectron angular distributions for the $P_{11}(5/2)$ and the $Q_{21}+R_{11}(33/2)$ rotational branch lines for $(1+1)$ REMPI via the A, $v'=0$ state are shown in Fig. 7. The angular distributions were fitted with terms up to $P_4(\cos\theta)$, which is the maximum order permitted for an overall two-photon process. Fitted coefficients for the scans in Fig. 7 and other $A \leftarrow X$, (0,0) rotational branch lines investigated in this work are given in Table II. Typical of all the branch lines studied, the angular data in Fig. 7 are well fit by a simple $1 + A_2P_2(\cos\theta)$ distribution appropriate for an unaligned excited state. Clearly this should not be the case, since one can show[21] that the relative $M_{J'}$ populations 3/2:1/2 produced via the $P_{11}(5/2)$ line are 1:1.5 and not 1:1 as would be required for an unaligned level. For higher J' levels, the alignment (as described by $A_0^{(2)}$) is expected to reach a limiting value[6,13] depending on branch, however, it remains nonzero in apparent contrast with alignments implied by the angular distributions given in Table II. Finally we note that for both the $(2+1)$ and $(1+1)$ REMPI of the E and A states, respectively, the A_2 coefficients of the photoelectron angular distributions are relatively insensitive to excitation branch and intermediate state J'.

IV. DISCUSSION

A. Limits on observable anisotropy in photoelectron angular distributions

As stated earlier, the only restriction on the angular distribution given by Eq. (4) which is independent of the internal structure of the target and the ionization dynamics is $k_{\max} = N$, where N is the total number of photons in the REMPI process. This constraint is simply a generalization of Yang's Theorem for multiphoton processes.[22] Observation of the full anisotropy given by $k_{\max} = N$ was realized for only a few rotational branch lines in the $(2+1)$ REMPI of the E, $v'=0$ state and not at all for a wide range of rotational levels probed in the $(1+1)$ REMPI of the A, $v'=0$ state. Previous $(n+1)$ REMPI photoelectron studies of NO[23–25] have resulted in nearly $\cos^2\theta$ distributions suggesting isotropic intermediate levels. In contrast, Pratt *et al.*[26] have

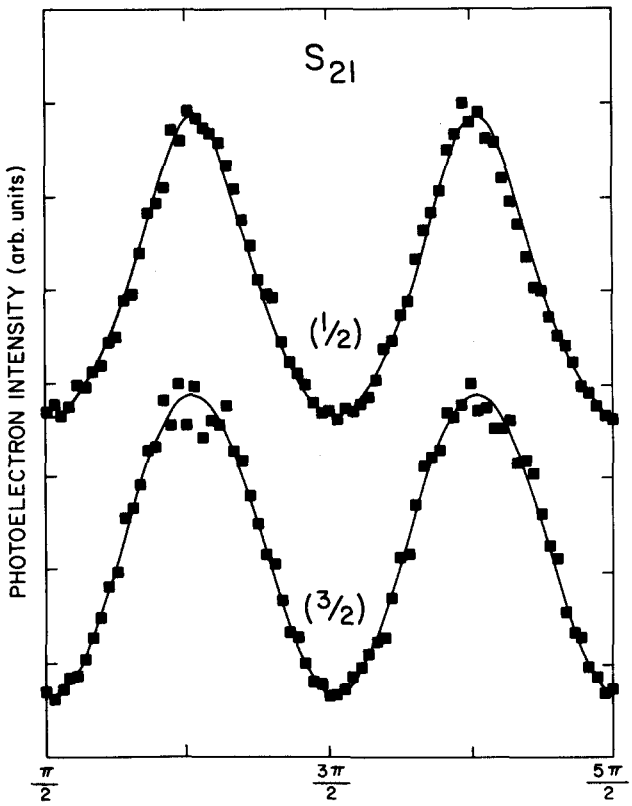

FIG. 6. Photoelectron angular distributions for $(2+1)$ REMPI of the $E\,^2\Sigma^+, v'=0$ state via the first two members of the S_{21} rotational branch. ■ experiment; — least squares fit to Eq. (4).

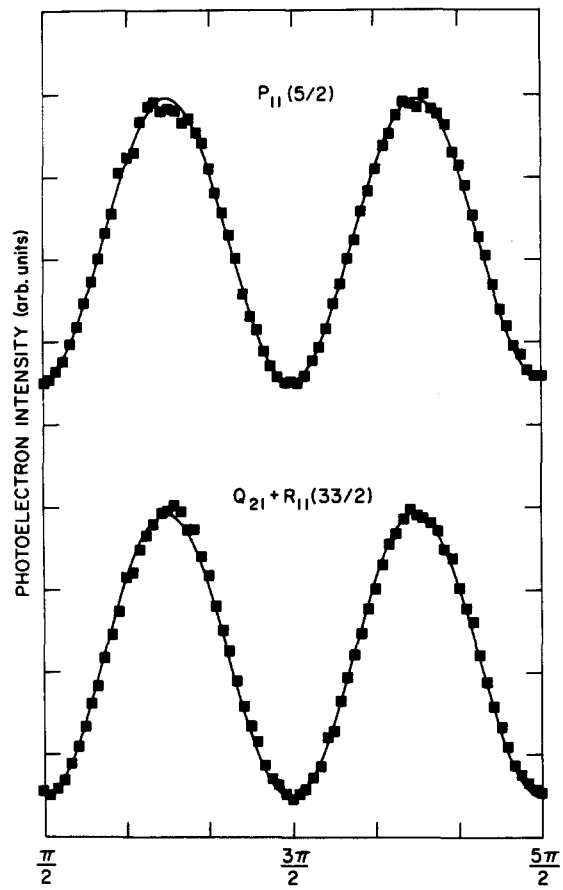

FIG. 7. Photoelectron angular distributions for $(1+1)$ REMPI of the $A\,^2\Sigma^+, v'=0$ state via low and high J'' rotational branch lines. ■ experiment; least-squares fit to Eq. (4).

observed significant deviations from $\cos^2\theta$ distributions in recent PES studies in $(3+1)$ REMPI of H_2. Clearly, additional constraints must be considered in order to rationalize the observed angular distributions.

Based on a general theoretical treatment of molecular REMPI, Dixit and McKoy[2] placed limits on the observable anisotropy based on angular momentum constraints imposed by the intermediate state and the ionization dynamics. In particular, they find for an $(n+1)$ REMPI process in which only one intermediate J' is populated and the rotational state of the ion is unresolved, that k_{max} is given by the smaller of $n+1, J'+1$, or l_{max}. Here l_{max} is the maximum orbital angular momentum component of the ejected photoelectron. This limitation on the maximum degree of anisotropy is the consequence of a simple physical effect, namely, that a diffuse angular distribution convolved by a highly anisotropic distribution will still be diffuse. The sum $J'+1$ (or $n+1$) gives the total anisotropy created in the final state (molecular ion plus photoelectron) from J' (or n) angular momenta in the intermediate state and one unit of angular momentum from the ionization photon. l_{max} reflects the maximum anisotropy the photoelectron can exhibit. The constraint $k_{max}=l_{max}$ also gives the close connection between the photoionization dynamics of the final step and the observed photoelectron angular distribution. In this regard, $(n+1)$ REMPI angular distributions can provide very much the same information as in conventional one-photon photoelectron spectroscopy. The negative aspect of this constraint is that higher order moments of the alignment $(A_0^{(4)}, A_0^{(6)}, \ldots)$ can only be "exposed" in such experiments if the outgoing continuum electron contains high $l(l>1)$ components. As a result, complex REMPI photoelectron angular distributions will only result when the intermediate level retains its excitation induced alignment and when the photoelectron is scattered into high l channels. Given the highly anisotropic nature of most molecular potentials, one would not expect the photoelectron continuum to be domi-

TABLE II. Fitted photoelectron angular distribution coefficients for $(1+1)$ REMPI of the $A\,^2\Sigma^+, v=0$ level of NO.

Rotational transition	A_2[a,b]
$P_{11}(3/2)$	1.24
$Q_{21}+R_{11}(3/2)$	1.38
$P_{12}(5/2)$	1.41
$P_{11}(5/2)$	1.35
$R_{22}(13/2)$	1.33
$R_{21}(23/2)$	1.33
$Q_{21}+R_{11}(27/2)$	1.44
$Q_{21}+R_{11}(29/2)$	1.39
$Q_{21}+R_{11}(31/2)$	1.39
$Q_{21}+R_{11}(33/2)$	1.40
$Q_{11}+P_{21}$(BH)	1.32

[a] Normalized coefficient $A_2=a_2/a_0$.
[b] An error of ± 0.05 is estimated for these coefficients.

nated by a few, low l channels except for the simplest systems such as H_2 or for high n Rydberg states in which the excited levels are reasonably well described by a single l value. In general, though, high l continua will be suppressed due to the increasing centrifugal barrier, thereby reducing the sensitivity of photoelectron spectroscopy to alignment effects.

Finally, the observation of higher order moments ($k \geqslant 2$) requires that the excited state population retain its spatial alignment in the time interval between excitation and ionization. Depolarization by gas collisions in the present studies is unlikely since the background pressures were kept low ($2\text{–}5 \times 10^{-5}$ Torr) and by the one-color nature of these measurements which would require an M_J-changing collision to occur within the 8 ns (FWHM) excitation/ionization laser pulse. The observation of nonzero Q values for two-photon excitation of the E state confirms that these levels remain aligned for a time on the order of their radiative lifetime even though the alignment is significantly reduced by hyperfine coupling (see Table I). Laser dependent effects such as saturation and coherence could also modify the expected alignment, the latter playing a role for mixed branches (e.g., $Q_{21} + R_{11}$) for which the spin components (F_1,F_2) of the A or E state are spectrally unresolved. Simultaneous excitation of these levels will create a time-dependent superposition of excited states characterized by a coherence time given by $\Delta E/\hbar$ where ΔE is the energy separation (spin-splitting constant, $\gamma = -86\,\mathrm{MHz}$[21]). A recent analysis[27] of this effect for $(1+1)$ REMPI via the A state showed that for small spin-splittings, $A_0^{(2)}$ strongly depends on the coherence lifetime. In general, however, coherence is not expected to completely depolarize the intermediate state and its effect is predicted[27] to be much less important as J' increases.

Saturation induced effects in molecular REMPI have been discussed in detail elsewhere.[2,28] Although our A state distributions would be expected to be the most susceptible due to the high cross section for one-photon absorption, a quadratic power dependence was obtained over the entire range of laser intensities used in this work. A much more limited power dependent study was conducted for the $(2+1)$ E state REMPI and no significant changes in the angular distributions were observed. In both cases, the laser intensities were kept below the level where broadening of the photoelectron peaks due to space charge was discernible. It has been estimated[29] that "Coulomb" broadening sets in with as few as 10^3–10^4 ionization events per laser pulse. At this relatively low excitation rate, it is unlikely that saturation will strongly influence the observed alignment.

B. $E\,^2\Sigma^+(4s\sigma)$, $v=0$ state

For the $R_{21} + S_{11}$ (1/2, 3/2, 5/2) and $S_{21}(1/2)$ rotational branch lines, we are able to observe the full anisotropy of the REMPI process given by $k_{\max} = 3$. Inclusion of Legendre polynomials up to $P_6(\cos\theta)$ in the fits of these angular distributions implies that the continuum electron has $l = 3$ contributions. Given that the Rydberg states of NO form well behaved and nearly atomic-like series converging to the ground state of the ion, one would expect that $l = 1$ ($\epsilon p\sigma$,$\epsilon p\pi$) partial waves would dominate the electron continuum since the E state is nominally an $l = 0$ ($4s\sigma$) bound state. In a detailed analysis of the observed quantum defects and intensities in the Rydberg state spectra of NO, Jungen[30] showed that the nd series are strongly mixed with the $(n+1)s$ Rydberg states. Hence, the $4s\sigma$ level contains a significant $3d\sigma$ ($l = 2$) character which is estimated by Jungen to be 41%. By including $l = 2$ components in the bound state description of the E state, it is easy to rationalize $l = 3$ ($\epsilon f\sigma$,$\epsilon f\pi$) contributions to the continuum electron.

The observed decrease in the contribution of higher order anisotropy (P_4,P_6) in the $R_{21} + S_{11}$ angular distributions as J'' increases from 1/2 to 5/2 is attributed to a decrease in spatial alignment of the resonantly excited level. This conclusion is supported by the experimental Q values which only reflect the excited state alignment and which exhibit a similar trend for increasing J'' (see Table I). Theoretical Q values without hyperfine coupling show a similar trend, yet, the predicted Q values are significantly higher than that observed experimentally. Inclusion of hyperfine depolarization lowers the theoretical Q values, however, the observed trend with increasing J'' is lost. For the $R_{21} + S_{11}$ (7/2) line higher order terms in the distribution are not evident suggesting an excited state alignment which is too small to be probed by photoelectron measurements. We note that the Greene–Zare hyperfine treatment used here for predicting fluorescence anisotropies is valid subject to certain restrictions.[6] Specifically, these predictions are rigorous only in the limit where the fluorescence lifetime greatly exceeds the precession period due to hyperfine coupling. The precession referred to here is that of **J** about **F**, where the nuclear spin **I** is added to **J**, the total angular momentum excluding nuclear spin, and **F** is the resultant angular momentum vector. In fact, the $Q_{21} + R_{11}(1/2)$ experimental Q value is intermediate between the calculated values that include or neglect hyperfine depolarization, suggesting that the limiting case is not valid for this system.

Similar PES asymmetry behavior is observed in the S_{21} branch except that higher order contributions to photoelectron angular distributions have the opposite sign and the change to a simple $\cos^2\theta$ distribution occurs abruptly at $J'' = 3/2$. The sign change of higher order terms in the $S_{21}(1/2)$ distribution relative to the $R_{21} + S_{11}$ (J'') measurements reflects the different M_J distributions produced via different branches.[3] More striking is the inconsistency between the LIF and photoelectron angular distribution results for the S_{21} branch. Specifically, the fluorescence Q values are roughly the same for both the $S_{21}(1/2)$ and $S_{21}(3/2)$ lines while the photoelectron measurements suggest that the $S_{21}(3/2)$ excitation yields an alignment which is smaller than can be detected by these measurements. A plausible explanation of this result is that the ionization dynamics strongly depend on the total angular momentum of the upper state. For case (b), coupled electronic states such as the Σ Rydberg states of NO, the total angular momentum J' primarily reflects the rotational angular momentum N' of the core ($J' = N' \pm 1/2$). The implication then is that ion core–photoelectron interactions at higher N' result in exchanges of angular momenta such that higher l components

of the continuum electron are suppressed. Such exchanges of angular momenta have been widely used to describe the photoionization dynamics of ground state atoms and molecules[31] and represent the interpretive basis of theoretical treatments of photoionization using multichannel quantum defect theory.[32] Furthermore, both the $S_{21}(3/2)$ and $R_{21}+S_{11}(5/2)$ lines access $N=3$ of the E state yet the latter exhibits complex angular behavior for a relatively small fluorescence anisotropy ($Q=2.8\%$), while the former results in a $\cos^2\theta$ distribution for a much larger observed excited state alignment ($Q=9.8\%$). Hence, the ionization dynamics are strongly branch dependent as well. A similar discrepancy is found for the $Q_{21}+R_{11}(1/2)$ line for which the observed anisotropy index ($Q=10.8\%$) suggests substantal alignment which is not borne out in the photoelectron angular distribution measurements (see Table I).

An interesting aspect of the results given in Table I is the near constant value of the A_2 coefficient obtained for all the branch lines independent of whether or not higher order terms are observed [A_2 (average) $=1.23\pm0.06$]. From a phenomenological point of view, this result suggests that the A_2 coefficient reflects primarily the photoionization dynamics of the isotropic E, $v'=0$ state and is relatively insensitive to the excitation induced alignment. Although this interpretation can only be tested by detailed calculations such as that recently completed by McKoy and co-workers, this result has particularly useful consequences. Specifically, photoelectron angular distributions from excited states can provide basic information on the energy dependent photoionization dynamics which can be interpreted or even calculated using existing model theories of photoionization without including laser dependent terms and the influence of excited state alignment. In this way, survey measurements of photoionization dynamics can be performed from a large number of initial states for which the experimenter can "select" the bound state properties to be probed, e.g., coupling case, Rydberg-valence mixing, etc.

C. $A\,^2\Sigma^+(3s\sigma)$, $v=0$ state

None of the rotational branch transitions studied for the A state exhibited significant deviation from a simple $\cos^2\theta$ distribution, even though very anisotropic M_J distributions are expected to result from one-photon excitation via linearly polarized light. Although hyperfine depolarization and coherent excitation of mixed branches can modify and decrease the alignment expected from simple angular momentum considerations, we interpret the lack of P_4 character in these angular distributions as resulting from the limitation imposed by l_{max}. Unlike the $4s\sigma(E)$ state, the $3s\sigma(A)$ state cannot interact with higher lying nd Rydberg levels, so that higher l components in the $3s\sigma(A)$ wave function are not likely to contribute significantly. This expectation is supported by bound state calculations which show the $3s\sigma$ wave function to be 94%–98% $s(l=0)$ type character.[7,33] A simple, atomic-like extension to photoionization from this state would lead to $p(l=1)$ continua which would result in $l_{max}=1$ and no observable P_4 character in the photoelectron angular distributions. In a recent theoretical study of $(1+1)$ REMPI via the A state, Dixit *et al.*[7] find that the outgoing $l=1$ partial wave can be scattered into a state of coupled l waves by interaction of the noncentral potential of the NO^+ ion core. In particular, they find that the $\epsilon\sigma$ ionization channel is dominated by the $f\sigma$ ($l=3$) component which they ascribe to the proximity of a shape resonance. An angular distribution calculation using these continuum functions for the $\Delta N=0$ component for an $R(21.5)$ transition results in significant P_4 character with $A_4/A_2=0.24$ (the $\Delta N=0$ ionization transition dominates $\Delta N=\pm1, 2$ transitions).[34] In contrast, our own results for high J'', R-branch lines [$R_{11}(13/2), R_{21}(23/2)$] do not exhibit significant P_4 character. It would appear from our data that either the contribution of the $l=3$ continua is overestimated in these calculations, or that the dynamical terms involving $l=3$ continua become negligibly small upon rotational averaging of the molecular ion. Further theoretical calculations are clearly needed to resolve the discrepancy raised by our experimental angular distributions.

Finally, we note that as found for the E state, the A_2 coefficients for all the A state branch lines studied are relatively constant with an overall average of $A_2=1.36\pm0.06$. Again, it is expected that this A_2 value reflects the overall ionization dynamics of the A, $v'=0$ state over the one-photon energy range spanned by these rotational transitions, independent of the excitation pathway and associated alignment.

ACKNOWLEDGMENTS

The authors wish to thank R. L. Dubs, Dr. S. N. Dixit, and Professor V. McKoy for providing their unpublished results on the E state fluorescence anisotropies and for helpful discussions. Research at Brookhaven National Laboratory was supported by the U. S. Department of Energy through its Office of Basic Energy Sciences, Division of Chemical Sciences under Contract No. DE-AC02-76CH00016. Research performed at Boston University was sponsored by the National Science Foundation (CHE-8310661) and the Air Force Office of Scientific Research, Air Force Systems Command, USAF (AFOSR-84-0261).

[1]Recent reviews are given in J. L. Dehmer, D. Dill, and A. C. Parr, in *Photophysics and Photochemistry in the Vacuum Ultraviolet*, edited by S. McGlynn, G. Findley, and R. Huebner (Reidel, Dordrecht, 1985); T. A. Carlson, M. O. Krause, J. W. Taylor, P. R. Keller, M. N. Piancastelli, F. A. Grimm, and T. A. Whitley, IEEE Trans. Nucl. Sci. **NS30**, 1034 (1983).
[2]S. N. Dixit and V. McKoy, J. Chem. Phys. **82**, 3546 (1985).
[3]R. L. Dubs, S. N. Dixit, and V. McKoy, J. Chem. Phys. **85**, 656 (1986).
[4]R. L. Dubs, S. N. Dixit, and V. McKoy, J. Chem. Phys. **85**, 6267 (1986).
[5]U. Fano and J. H. Macek, Rev. Mod. Phys. **45**, 553 (1973).
[6]C. H. Greene and R. N. Zare, J. Chem. Phys. **78**, 6741 (1983); Annu. Rev. Phys. Chem. **33**, 119 (1982).
[7]S. N. Dixit, D. L. Lynch, V. McKoy, and W. M. Huo, Phys. Rev. A **32**, 1267 (1985).
[8]P. Lambropoulos, Adv. At. Mol. Phys. **12**, 87 (1976).
[9]M. P. Strand, J. Hansen, R.-L. Chien, and R. S. Berry, Chem. Phys. Lett. **59**, 205 (1978).
[10]S. N. Dixit and P. L. Lambropoulos, Phys. Rev. Lett. **46**, 1278 (1981); Phys. Rev. A **27**, 168 (1983).
[11]J. Cooper and R. N. Zare, J. Chem. Phys. **48**, 942 (1968).
[12]Reference 1 and references therein.
[13]W. J. Kessler and E. D. Poliakoff, J. Chem. Phys. **84**, 3647 (1986).

[14]K.-M. Chen and E. S. Yeung, J. Chem. Phys. **70**, 1312 (1979).
[15]M. Dubs, U. Bruhlman, and J. R. Huber, J. Chem. Phys. **84**, 3106 (1986).
[16]A. C. Kummel, G. O. Sita, and R. N. Zare, J. Chem. Phys. **85**, 6879 (1986).
[17]R. L. Dubs, S. N. Dixit, and V. McKoy, unpublished results.
[18]K. P. Huber and G. Herzberg, *Constants of Diatomic Molecules* (Van Nostrand Reinhold, New York, 1979).
[19]E. Miescher, Can J. Phys. **49**, 2350 (1971).
[20]J. B. Halpern, H. Zacharias, and R. Wallenstein, J. Mol. Spectrosc. **79**, 1 (1980).
[21]D. C. Jacobs, R. J. Madix, and R. N. Zare, J. Chem. Phys. **85**, 5469 (1986), Eq. (4).
[22]C. N. Yang, Phys. Rev. **74**, 764 (1948).
[23]Y. Achiba, K. Sato, K. Shotabake, and K. Kimura, J. Chem. Phys. **78**, 5474 (1983).
[24]M. G. White, W. A. Chupka, M. Seaver, A. Woodward, and S. D. Colson, J. Chem. Phys. **80**, 678 (1984).
[25]J. C. Miller and R. N. Compton, J. Chem. Phys. **84**, 675 (1985).
[26]S. T. Pratt, P. M. Dehmer, and J. L. Dehmer, J. Chem. Phys. **85**, 3379 (1986).
[27]J. R. Appling, M. G. White, R. L. Dubs, S. N. Dixit, and V. McKoy, J. Chem. Phys. **87**, 6927 (1987).
[28]D. C. Jacobs and R. N. Zare, J. Chem. Phys. **85**, 5457 (1986).
[29]J. T. Meek, S. R. Long, and J. P. Reilly, J. Phys. Chem. **86**, 2809 (1982).
[30]Ch. Jungen, J. Chem. Phys. **53**, 4168 (1970).
[31]D. Dill, in *Photoionization and Other Probes of Many-Electron Interactions*, edited by F. J. Wuilleumier (Plenum, New York, 1976), p. 387.
[32]K. T. Lu, in *Photophysics and Photochemistry in the Vacuum Ultraviolet*, edited by S. P. McGlynn, G. L. Findley, and R. H. Huebner (Reidel, New York, 1985), p. 217.
[33]V. S. Viswanathan, E. Sekreta, E. R. Davidson, and J. P. Reilly, J. Chem. Phys. **90**, 5078 (1986).
[34]W. G. Wilson, K. S. Viswanathan, E. Sekreta, and J. P. Reilly, J. Phys. Chem. **88**, 672 (1984).